Available online at www.sciencedirect.com

SciVerse ScienceDirect

journal homepage: www.elsevier.com/locate/he

Effect of electrolyte concentration on the electrochemical properties of an AB5-type alloy for Ni/MH batteries

F.C. Ruiz [a,b,*], P.S. Martínez [a], E.B. Castro [b,c], R. Humana [c], H.A. Peretti [a], A. Visintin [b,c]

[a] Centro Atómico Bariloche (CAB), Comisión Nacional de Energía Atómica (CNEA), Av. Bustillo 9500, C. P. 8400, S. C. de Bariloche, RN, Argentina

[b] CONICET Consejo Nacional de Investigaciones Científicas y Técnicas, Av. Rivadavia 1917, C1033AAJ Ciudad de Buenos Aires, Argentina

[c] Instituto de Investigaciones Fisicoquímicas, Teóricas y Aplicadas, Universidad Nacional de La Plata, Diagonal 113 y calle 64, Suc. 4, C.C. 16, Comisión de Investigaciones Científicas Provincia de Buenos Aires (C.I.C.), CP 1900, La Plata, Argentina

ARTICLE INFO

Article history:
Received 24 May 2012
Received in revised form
14 September 2012
Accepted 2 October 2012
Available online 20 November 2012

Keywords:
Battery
Alloy
Hydride
Energy
Electrolyte

ABSTRACT

This publication is the first of a series of three that we have undertaken to study the effect of electrolyte concentration on electrode performance. Here, the electrochemical properties of an AB_5-type alloy, namely $LaNi_{3.6}Co_{0.7}Mn_{0.4}Al_{0.3}$, are investigated using different KOH electrolyte concentrations (i.e. 2 M, 4 M, 6 M and 8 M). The next two publications will be concerned with an AB_2-type alloy and a Mg-based alloy, respectively.

From the present study, the 6 M and 8 M electrodes were those that exhibited faster activation, maximum discharge capacity values (~325 mAh/g) and best performance under high-rate dischargeability. Nevertheless, the capacity loss rate increased as KOH concentration augmented.

The electrochemical behavior is analyzed in terms of a physicochemical model based on the theory of porous electrodes. The fitting of electrochemical impedance spectroscopy data in terms of the model allowed determining kinetic parameters of the hydriding reaction, transport of hydrogen in the alloys and structural electrode parameters.

1. Introduction

Nickel-metal hydride rechargeable batteries (Ni/MH) are used in a wide range of electrical devices, from mobile devices such a digital camera to hybrid electric vehicle (HEV), including cellular phones, electric toys, robots, etc [1–7].

A Ni/MH battery consists of an assembly of a hydride-forming alloy (negative electrode) and a nickel oxyhydroxide, NiOOH, (positive electrode) immersed in a 6 M KOH electrolyte, separated by an adequate separator. In this molar concentration, the solution provides the highest ionic conductivity for use in Ni/MH [8], but is a very aggressive environment, promoting corrosion in the hydride-forming alloy. An electrolyte with a lower concentration of KOH decreases the corrosion processes – improving the cycle life – and reduces costs. However, the decrease in concentration of KOH leads to the reduction of electrical conductivity of the electrolyte. Nevertheless, there are few scientific works about the influence of this high concentration of the electrolyte used in Ni/MH batteries. Song et al. [9] studied this influence in the perovskite-type oxide $LaCrO_3$ using KOH electrolyte in the 5.6–12.5 M range, finding that capacity increases as KOH

* *Corresponding author*. Centro Atómico Bariloche (CAB), Comisión Nacional de Energía Atómica (CNEA), Av. Bustillo 9500, C. P. 8400, S. C. de Bariloche, RN, Argentina. Tel.: +54 2944 44 5271; fax: +54 2944 445190.
E-mail address: ruizfabricio@yahoo.com.ar (F.C. Ruiz).
0360-3199/$ – see front matter
http://dx.doi.org/10.1016/j.ijhydene.2012.10.007

concentration is augmented. Also, Guiose et al. analyzed the electrochemical performance of an AB_2 alloy using KOH 6 M and 8 M, finding that electrolyte concentration affects the activation, which shortens with increasing KOH concentration. However, the alloy degradation in 8 M was faster than 6 M [10]. Khaldi et al. reported a noticeable improvement in the electrochemical properties using a KOH 1 M against 8 M concentration electrolyte in AB_5 alloy [11]. The obtained results for Khaldi et al. are contrary to expectations.

In this context, a systematic study about the influence of KOH electrolyte concentration in different alloy types is necessary to clarify aspects related to this issue.

In this work, electrochemical measurements employing different KOH concentrations were performed using an AB_5-type alloy. The material was designed and elaborated in our laboratory, and was analyzed structural and electrochemically. Properties such as electrochemical capacity, activation processes and high-rate dischargeability (HRD) were investigated. Also, electrochemical impedance spectroscopy (EIS) measurements were performed. The best electrode performance was obtained with 6 M and 8 M KOH concentrations.

2. Experimental

An AB_5-type alloy of target composition $LaNi_{3.6}Co_{0.7}Mn_{0.4}Al_{0.3}$ was prepared by arc melting adequate proportions of the composition elements (purity better than 99.9%) inside a copper-cooled hearth under high purity argon (99.998%). In order to improve the purity of the melting atmosphere, a sacrifice button of Zr was melted previously. The resulting alloy button (of about 30 g) was turned over and remelted at least two times to assure homogeneity.

EDS and XRD techniques were used for the metallurgical characterization of the alloy.

For the electrochemical characterization, electrodes were prepared by compacting a mixture of 100 mg of alloy particles (74 μm < size particle < 125 μm) with equal amounts of teflonized carbon powder (Vulcan XC-72), using a cylindrical die and a pressure of 1900 kg/cm^2 at 20 °C. The resulting electrode has a surface of 2 cm^2 and a thickness of 1 mm. A Ni wire was used as current collector. The electrochemical measurements were carried out using four electrochemical cells with different solutions (KOH 2 M, 4 M, 6 M and 8 M) at room temperature. A Ni mesh was employed as counter-electrode, and Hg/HgO as reference electrode. The galvanostatic charge–discharge technique was applied. A constant cathodic current of 100 mA/g during 4.5 h was used to assure the full charge of the working electrode. The discharge was conducted at 100 mA/g (anodic current) until the cutoff potential of −0.6 V was reached. Electrochemical impedance spectroscopy (EIS) and high-rate dischargeability (HRD) techniques were performed when the electrochemical cells reached 70 charge–discharge cycles.

An Autolab PGSTAT 30 potentiostat was employed for EIS and HRD measurements. EIS determinations were performed in the 0.5 mHz–65 kHz frequency range with a sine signal amplitude of 6 mV. The discharge currents used for HRD were 20, 50, 100, 200, 500 and 1000 mA/g.

3. Results and discussion

3.1. Metallurgical characterization

The X-ray energy-dispersive spectroscopy spectrum of the AB_5 alloy is presented in Fig. 1, whereas in Table 1 the obtained values of the EDS analysis (ov) and the target composition values (tv) are shown, for comparison. As observed in this table, a good agreement is obtained between determined and target composition values.

In Fig. 2, the X-ray diffraction pattern of the alloy is shown. This pattern can be indexed well assuming the $CaCu_5$-type structure with hexagonal symmetry and the P6/mmm space group [12,13]. It can be seen that all diffraction peaks correspond to the typical AB_5-type alloy structure. The lattice parameter values were calculated using the XRD data. The obtained values were $a = 5.03$ nm and $c = 3.97$ nm. These results are in good agreement with the obtained results in Refs. [12,13].

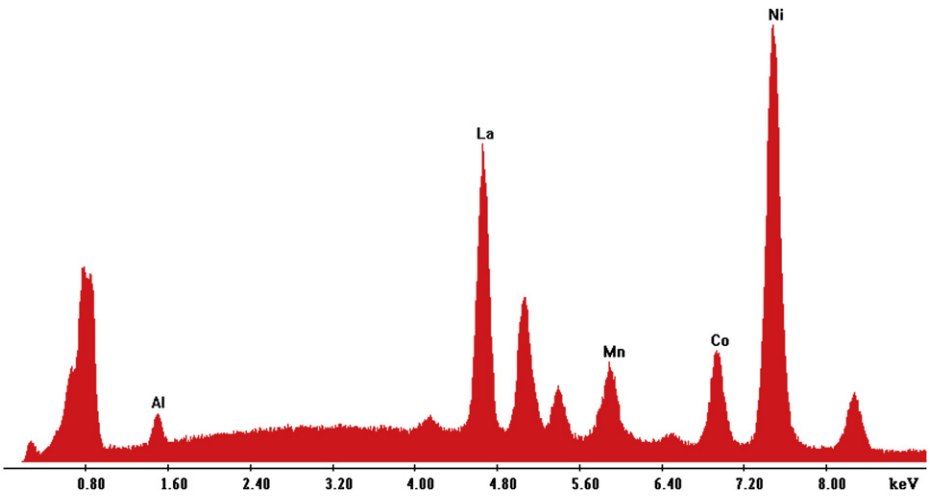

Fig. 1 – EDS spectrum of the $LaNi_{3.6}Co_{0.7}Mn_{0.4}Al_{0.3}$ alloy.

Table 1 – Composition values obtained by EDS technique in comparison with target values.

	La	Ni	Co	Mn	Al
at. % ov	17.9	57.6	11.7	6.6	6.2
at. % tv	16.7	60.0	11.6	6.7	5

3.2. *Electrochemical characterization*

The relationship between the discharge capacity and charge–discharge cycles is shown in Fig. 3. The maximum discharge capacity obtained was 325 mAh/g, corresponding to cells containing KOH 6 M and 8 M.

All samples present fast activation, being this fact a typical characteristic of AB_5-type alloys. Cells containing KOH 6 M and 8 M solutions present the best performance, regarding this process.

Also, the discharge capacity decreases for all samples with charge–discharge cycling.

In Table 2, capacity loss rate is shown for all samples. These values were obtained from the slope of the linear part of the capacity curve, taking the cycle corresponding to the maximum capacity as a starting point.

HRD measurements, in absolute and relative values, are shown in Fig. 4. The relative values were calculated taking as reference the maximum discharge capacity measured with 20 mA/g discharge current.

The working electrode corresponding to KOH 6 M electrolyte presents an excellent performance, obtaining around 90% of maximum capacity with a 3 C-rate (discharge current ≈ 900 mA/g).

The HRD performance decreases as follows: 6 M > 8 M > 4 M > 2 M.

The activation process and HRD performance are related to kinetic processes. In these processes, the electrical conductivity of the electrolyte plays a fundamental role. This conductivity is maximum at 6 M KOH [8]. Nevertheless, it is observed a decrease in the discharge capacity as electrolyte concentration rises. This fact can be related to the oxidation processes, which are favored with higher electrolyte concentrations. This is an important aspect in which an electrolyte low concentration can improve the electrochemical properties of the hydride alloys. This aspect could be more relevant for the AB_2-type alloys, due to the difficult activation processes that exhibit these alloys.

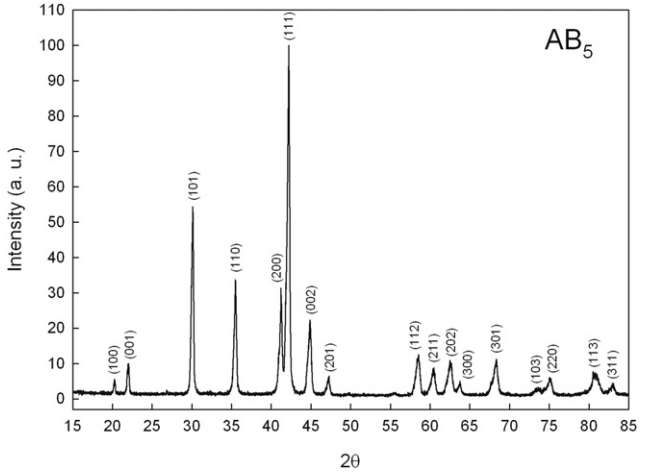

Fig. 2 – $LaNi_{3.6}Co_{0.7}Mn_{0.4}Al_{0.3}$ alloy XRD pattern.

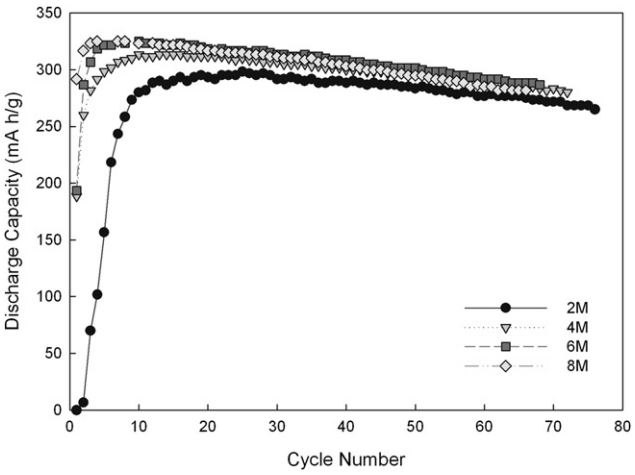

Fig. 3 – Discharge capacity of $LaNi_{3.6}Co_{0.7}Mn_{0.4}Al_{0.3}$ vs. charge–discharge cycles number for all samples.

3.3. *Impedance results and physicochemical model*

In Fig. 5, Nyquist diagrams corresponding to the impedance response of the electrodes, with different KOH concentrations, are presented. EIS measurements correspond to 50% state of charge (SOC), then $X = 0.5$. The diagrams show a high frequency response, with a phase angle close to 45°, characteristic of a porous structure. The capacitive loop in the range of intermediate frequencies is associated with the parallel connection of the electrical double layer, C, with the charge transfer resistance, R_t, related to the hydrogen absorption/desorption process on the surface of the alloy particles. From the figure it is evident that R_t decreases as KOH concentration increases. In the low frequencies region, a Warburg type response, associated to the hydrogen diffusion process, is observed.

The EIS response of the system was analyzed in terms of a physicochemical model [14], in which the porous nature of the electrode material is taken into account, considering infinite electronic conductivity in the solid phase and an average particle size [15]. The hydrogen absorption/desorption processes, taking place at the surface of the alloy particles, are described in terms of a kinetic scheme including hydrogen absorption coupled to hydrogen diffusion into the electrode material.

The impedance function of the porous structure, Z_p, may be expressed as:

Table 2 – Capacity loss rate (in mAh/g) per cycle.

2 M	4 M	6 M	8 M
0.5216	0.5274	0.6582	0.7707

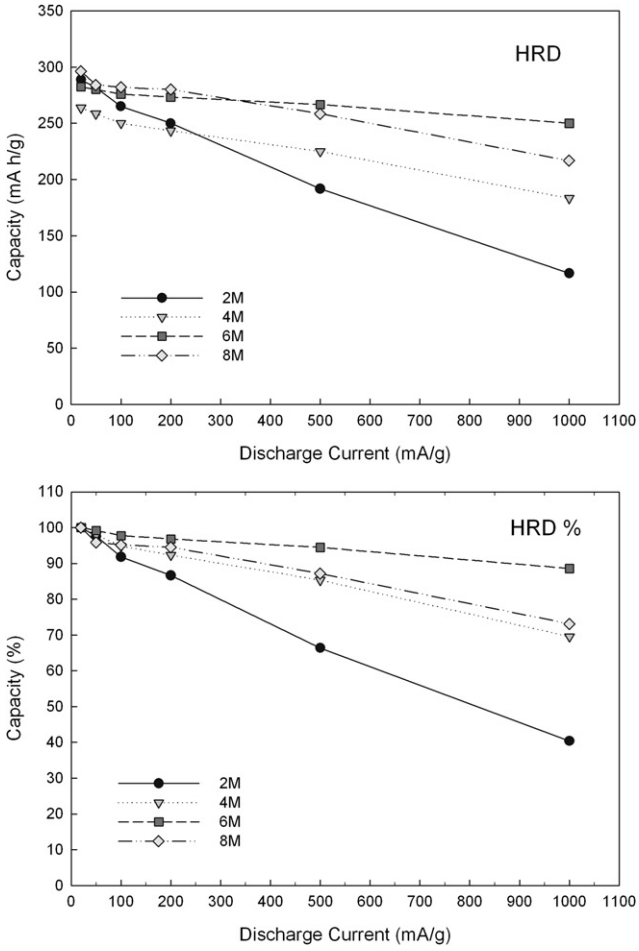

Fig. 4 – HRD measurements of all samples, in absolute and relative values.

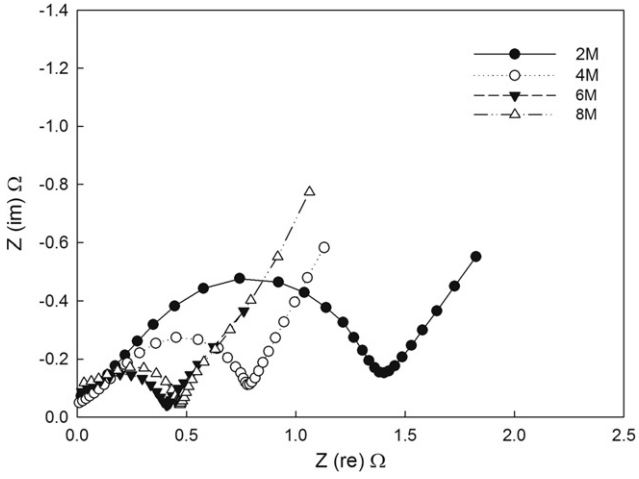

Fig. 5 – Nyquist diagrams for AB_5 electrodes with different KOH concentrations (50% SOC).

$$Z_p = R_i + \frac{L_e}{A_p k}\frac{\cosh(\nu)}{\nu \sinh(\nu)} \quad (1)$$

where:

$$\nu = \sqrt{\omega C + \frac{1}{Z_f}} \quad (2)$$

$$C = \frac{C_{dl} A_i L_e^2}{k} \quad (3)$$

$$Z_f = R_t + \frac{A}{\sqrt{\omega}} \quad (4)$$

$$\frac{1}{R_t} = \frac{i_o F A_a L_e^2}{RTk} \quad (5)$$

$$A = \frac{RTk}{L_e F^2 C_{max} A_a X(1-X)\sqrt{D}} \quad (6)$$

The theoretical impedance plots included in Fig. 6 were calculated using eqs. (1)–(6). For the identification of the parameters of the system, a fitting procedure based on the

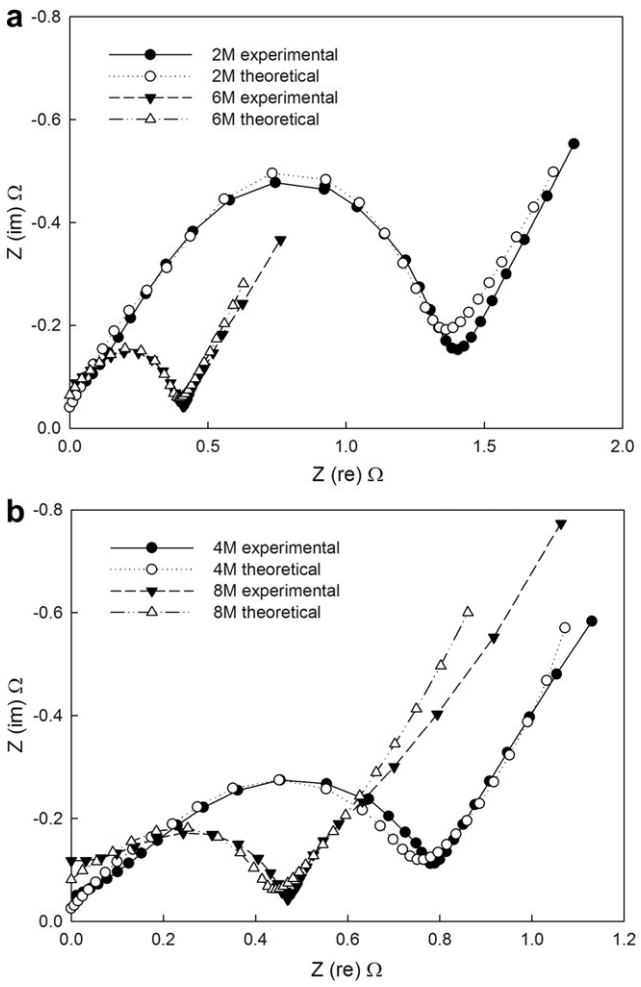

Fig. 6 – EIS data: simulated and experimental Nyquist plots. a) KOH concentration 2 M and 6 M, b) KOH concentration 4 M and 8 M (presented in this way for a good visualization).

Table 3 – Parameters values derived from the fitting procedure, for AB_5 alloy electrodes with different concentration.

	2 M KOH	4 M KOH	6 M KOH	8 M KOH
i_o (A/cm$^{2)}$	0.00053	0.0010	0.0018	0.001728
A_i (cm^{-1})	225,198	204,788	93,947.6	57,266.8
k (S/cm)	0.100	0.183	0.225	0.224
k_0 (S/cm)	0.371	0.579	0.651	0.626
A_a (cm^{-1})	403.6	394.6	424.7	359.8
D (cm^2/s)	1×10^{-10}	1×10^{-10}	1×10^{-10}	1×10^{-10}

Nelder–Meade simplex search algorithm [16] was implemented. An analysis of the identifiability of the parameters in eq. (1), indicates that i_o may be identified from R_t (eq. (5)), if the parameter A_a is known. Accordingly A_a was identified from A (eq. (6)), assuming $D = 1 \times 10^{-10}$ cm^2/s and $C_{max} = 0.06$ mol/cm^3 [14]. The parameters derived from the fitting procedure are displayed in Table 3.

According to the proposed kinetic mechanism, the exchange current density i_o is given by the function of eq. (7) [17]

$$i_o = i^0_{ref}\left(\frac{c_{ref}}{c}\right)^{\alpha c}\left(\frac{1-x}{1-x_{ref}}\right)^{\alpha a}\left(\frac{x_{ref}}{x}\right)^{\alpha c}\left(\frac{c_{H_2O}}{c_{H_2O_{ref}}}\right)^{\alpha a} \quad (7)$$

Fig. 7 depicts the logarithmic dependence of i_o with c. From the slope of the plot, the cathodic transfer coefficient, α_c, may be derived, corresponding to $\alpha_c = -0.9$.

The fitting procedure allowed the identification of the effective conductivity of the electrolyte (k). From Table 3, it is evident that k increases when the concentration electrolyte is augmented, presenting a maximum at 6 M. As shown in Fig. 8, the same trend is observed for k_o, calculated in terms of eq. (8) [18], which relates the conductivity of the electrolyte with concentration.

$$k_0 = -7.593x10^{-3} + 2.3831x10^2 c - 2.5997x10^4 c^2 + 7.6442x10^5 c^3 - 9.6275c^4 (S/cm) \quad (8)$$

k has been related to k_o through [18]:

$$k = k_0 \varepsilon^{\tau} \quad (9)$$

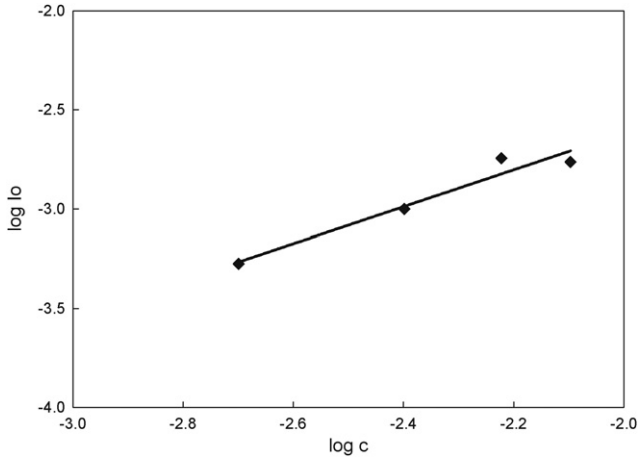

Fig. 7 – Logarithmic dependence of i_o with electrolyte concentration.

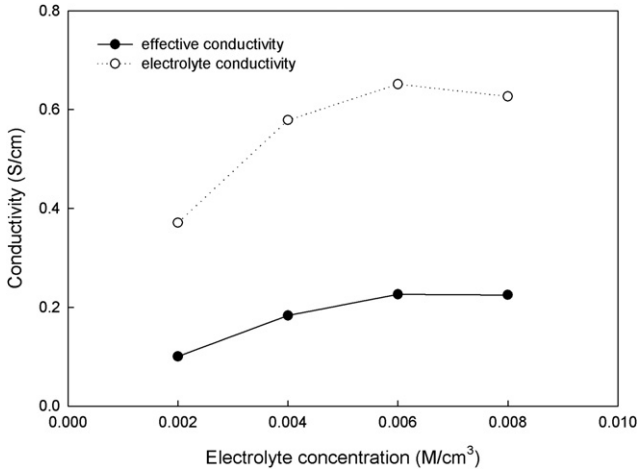

Fig. 8 – Conductivity vs. concentration electrolyte.

being ε the porosity of the electrode and τ a tortuosity parameter ($\tau = 1$). According to eq. (8) and Table 3, porosity values from 27% to 35% were obtained.

4. Conclusions

AB_5 alloy elaboration was achieved satisfactorily, as deduced from the obtained XRD and EDS results.

All electrodes show a fast activation and a decrease in the electrochemical capacity with increasing number of charge/discharge cycles. The maximum capacity value corresponds to KOH concentration 6 M and 8 M. Similarly, KOH concentration 6 M and 8 M present the best performance in HRD.

The capacity loss rate increases with increasing KOH concentration.

The analysis of EIS data indicates an increase of i_o with KOH concentration, in accordance with the proposed dependence of eq. (6). The dependence of the effective conductivity (k) with electrolyte concentration (c) also agrees with the theoretical prediction.

The dependence of i_o and k with the KOH concentration, predicted by the model, allows to explain the HRD behavior of the system, being the 6 M KOH electrolyte the one exhibiting the best performance. This is due to the fact that though the kinetic overpotential (inversely proportional to I_0, Fig. 7) diminishes with increasing KOH concentration, the ohmic overpotential (inversely proportional to the conductivity, Fig. 8) shows a minimum at 6 M KOH.

The electrolyte optimum concentration, according to measurements made in this work, is KOH 6 M for the AB_5 alloy. However, the loss rate capacity decreases when the KOH concentration increases.

Glossary

Z_p	electrode impedance, Ω
R_i	ohmic resistance, Ω
L_e	electrode thickness, cm

A_p	geometric area of the electrode, cm^2
k	effective conductivity, S/cm
k_o	electrolyte conductivity, S/cm
ω	frequency, s^{-1}
C_{dl}	double layer capacity, F
A_i	specific interfacial area, cm^2/cm^3
R_t	charge transfer resistance, Ω
R	gas constant, J/K mol
T	temperature, K
F	faraday constant, coulomb
c	electrolyte concentration
c_{H_2O}	water concentration
C_{max}	max. concentration of H in the alloy, mol/cm^3
X	fractional concentration of H in the alloy (state of charge)
A_a	specific active area, cm^2/cm^3
D	diffusion coefficient, cm^2/s

REFERENCES

[1] Hariprakash B, Shukla AK, Venugoplan S. Secondary batteries – nickel systems | nickel–metal hydride: overview. In: Garche J, editor. Encyclopedia of electrochemical power sources. Elsevier; 2009. p. 494–501.

[2] Yang K, Wu F, Chen S, Zhang C. Effect of surface modification of metal hydride electrode on performance of MH/Ni batteries. T Nonferr Metal Soc 2007;17(1):200–4.

[3] Yang M, Nan J, Hou X, Li W. Preparation and electrochemical performances of nickel metal hydride batteries with high specific volume capacity. Chin J Chem Eng 2008;16(6):944–8.

[4] Begum SN, Muralidharan VS, Basha CA. Electrochemical investigations and characterization of a metal hydride alloy ($MmNi_{3.6}Al_{0.4}Co_{0.7}Mn_{0.3}$) for nickel metal hydride batteries. J Alloy Compd 2009;467(1–2):124–9.

[5] Srivastava S, Upadhyay RK. Investigations of AB_5-type negative electrode for nickel-metal hydride cell with regard to electrochemical and microstructural characteristics. J Power Sources 2010;195(9):2996–3001.

[6] Liu Y, Pan H, Gao M, Li R, Wang Q. Intrinsic/extrinsic degradation of Ti–V-based hydrogen storage electrode alloys upon cycling. J Phys Chem C 2008;112(42):16682–90.

[7] Shangguan E, Chang Z, Tang H, Yuan X, Wang H. Regulation of the discharge reservoir of negative electrodes in Ni–MH batteries by using $Ni(OH)_x$ ($x = 2.10$) and γ-CoOOH. J Power Sources 2011;196(18):7791–6.

[8] See DM, White RE. Temperature and concentration dependence of the specific conductivity of concentrated solutions of potassium hydroxide. J Chem Eng Data 1997;42:1266–8.

[9] Song M, Chen Y, Tao M, Wu C, Zhu D, Yang H. Some factors affecting the electrochemical performances of $LaCrO_3$ as negative electrodes for Ni/MH batteries. Electrochim Acta 2010;55(9):3103–8.

[10] Guiose B, Cuevas F, Décamps B, Leroy E, Percheron-Guégan A. Microstructural analysis of the ageing of pseudo-binary (Ti, Zr)Ni intermetallic compounds as negative electrodes of Ni–MH batteries. Electrochim Acta 2009;54(10):2781–9.

[11] Khaldi C, Mathlouthi H, Lamloumi J. A comparative study of 1 M and 8 M KOH electrolyte concentrations, used in Ni–MH batteries. J Alloy Compd 2009;469(1–2):464–71.

[12] Seo C, Choi S, Choi J, Park C, Lee J. Effect of V and Zr on the electrochemical properties of La-based AB_5-type metal hydride electrodes. J Alloy Compd 2003;351(1–2):255–63.

[13] Ma J, Pan H, Chen C, Wang Q. Effect of heat treatment on the microstructure and electrochemical properties of AB_5-type $MlNi_{3.60}Co_{0.85}Mn_{0.40}Al_{0.15}$ hydride alloy: 1.—the microstructure and P–C isotherms. Int J Hydrogen Energy 2002;27(1):57–62.

[14] Visintin A, Castro EB, Real S, Triaca WE, Wang C, Soriaga MP. Electrochemical activation and electrocatalytic enhancement of a hydride-forming metal alloy modified with palladium platinum and nickel. Electrochim Acta 2006;51:3658–67.

[15] Meyers JP, Doyle M, Darling RM, Newman J. The impedance response of a porous electrode composed of intercalation particles. J Electrochem Soc 2000;147:2930.

[16] Ruiz FC, Castro EB, Peretti HA, Visintin A. Study of the different ZrxNiy phases of Zr-based AB2 materials. Int J Hydrogen Energy 2010;35(18):9879–87.

[17] Paxton B, Newman J. Modeling of nickel/metal hydride batteries. J Electrochem Soc 1997;144(11):3818–31.

[18] Mao Z, De Vidts P, White RE, Newman J. Theoretical analysis of the discharge performance of a $NiOOH/H_2$ cell. J Electrochem Soc 1994;141:54–64.